



Research on the Rotor-Stator Interaction of Centrifugal Pump based on Sinusoidal Tubercle Volute Tongue

P. F. Lin, P. F. Song, Z. C. Zhu and X. J. Li[†]

Key Laboratory of Fluid Transmission Technology of Zhejiang Province, Zhejiang Sci-Tech University, Hangzhou, 310018, China

[†]Corresponding Author Email: lixj@zstu.edu.cn

(Received June 10, 2020; accepted July 26, 2020)

ABSTRACT

The rotor-stator interaction between the impeller and the volute is the main reason for the pump pressure pulsation and vibration. This work aims at designing a new type of tongue to minimize pressure pulsation, reduce vibration noise and energy loss. Inspired by the humpback pectoral fin, four volute tongues are investigated in this paper, three of which are sinusoidal tubercle volute tongues (STVT) and one is the original volute tongue (OVT). Based on the detached-eddy simulation (DES) turbulence model, the influence of the sinusoidal tubercle volute tongues on the pressure pulsation was investigated, and the flow structure and enstrophy of the four pumps were analyzed, aiming to minimize pressure pulsation, maximize hydraulic performance and reduce the energy dissipation in centrifugal pumps. The results show that the pressure pulsations of the STVT profiles are all lower. The reductions of the average pressure pulsation at the monitoring points are 13.3% (STVT-1), 20.6% (STVT-2), and 16.2% (STVT-3), respectively. The difference in pressure pulsation at the monitoring points closer to the tongue is more obvious. At the design flow rate, the efficiencies of the three bionic pumps are increased by 0.5% (STVT-1), 1.5% (STVT-2), 0.9% (STVT-3), respectively. The STVT profiles change the vortex structure near the tongue and minimized the vortex strength. Meanwhile, the flow in the pump with the STVT profiles have lower enstrophy. The enstrophy of the flow with the STVT-2 profile is the lowest, which is reduced by about 8%. This reduces the dissipation of mechanical energy. The results can be used as a guide for pump design optimization.

Keywords: Pressure pulsations; Centrifugal pump; Volute tongue; Bionics; Enstrophy.

NOMENCLATURE

A	the amplitude of the sinusoid	Δp	static pressure coefficient
b_2	blade width at exit	Q	actual flow rate
b_3	inlet width of volute	Q_d	designed flow rate
C	the width of the volute tongue	r^*	non-dimensional radial distance
C_p	pressure coefficient	r_{TE}	blade tip radius
d_1	inlet diameter of impeller	STVT	sinusoidal tubercle volute tongue
d_2	outlet diameter of impeller	T	time of one cycle of pump
d_3	volute tongue diameter	V_ω	angular velocity of the pump
H	pump head	V_r^*	non-dimensional radial velocity
L	the length of the longitudinal extension length	V_θ^*	non-dimensional circumferential velocity
OVT	original volute tongue	u_2	circumferential velocity at the impeller exit
p_{inlet}	static pressure of inlet	Z	blade number
p	static pressure		
\bar{p}	time average static pressure	β_2	blade angle at exit
p_i	pressure sample values	η	efficiency

θ	angular coordinate	ψ^*	head coefficient
λ	the sinusoidal wavelength	Ω	total enstrophy
ρ	density	Ω^*	enstrophy per unit volume
φ_d	nominal flow coefficient	ω	vorticity
ψ_n	nominal head coefficient		

1. INTRODUCTION

The centrifugal pump is a piece of important conveying equipment in the petroleum, thermal power generation, nuclear power generation, and other industries. The performance of pumps is closely linked to production efficiency. The vibration noise induced by the pressure pulsation in the centrifugal pump will not only affects the environment but also hinders the stable operation of the equipment. Therefore, reducing the pressure pulsation and improving the performance of the pump is important to the overall efficient operation of the system.

At present, there are many pieces of literature on the rotor-stator interaction phenomena in centrifugal pumps. In centrifugal pumps, due to the rotor-stator interaction between the impeller blades and the volute tongue, the flow had the characteristics of pressure fluctuations and uneven pressure distribution (Majidi, 2005). Especially in the vicinity of the impeller outlet and near the tongue pressure fluctuations were large (Spence and Amaral-Teixeira, 2008; Xiao *et al.* 2012). In order to minimize the pressure pulsation and energy dissipation caused by the rotor-stator interaction, a lot of analysis and research had been carried out. Changing the shape of the volute tongue, the tongue angles, and the exit area of the impeller would affect the pressure pulsation (Luo *et al.* 2013; Si *et al.* 2016; Zhang *et al.* 2015; Spence and Amaral-Teixeira, 2009). The addition of splitter blades had a significant effect on reducing pressure pulsation in the pipeline in centrifugal pumps (Solis *et al.* 2011; Kergourlay *et al.* 2007; Ye *et al.* 2012). Khalifa *et al.* (2011) found that the gap between the impeller and the volute was one of the main reasons affecting the pressure pulsation. By optimizing the gap, the purpose of reducing pressure pulsation and controlling vibration could be achieved. Shim *et al.* (2016) proposed a three-objective function optimization method to optimize the design of the double volute centrifugal pumps. Thus, the pressure pulsation and radial force were minimized and the hydraulic loss was small. Gao *et al.* (2016) analyzed the influence of five typical blade trailing edges on pressure pulsation and centrifugal pump performance. The results showed that a suitable blade trailing edge had a positive effect on reducing pressure pulsations. Different diffuser vane numbers would also affect the impeller blade passing frequency, and a lower diffuser vane number was beneficial to minimize the pressure fluctuation intensity (Bai *et al.* 2019).

In recent years, the application of bionics had attracted more and more attention of the researchers (Xue *et al.* 2016; Hua *et al.* 2019; Yang *et al.* 2017; Gu *et al.* 2019; Cheng *et al.* 2020; Huang *et al.* 2019). Some sinusoidal tubercles are growing in the pectoral fins of humpback, which allows them to move freely in the ocean. Shi *et al.* (2016) designed a tidal turbine blade with the leading-edge tubercles by using this feature. The results showed that the bionic blade improves the lift-to-drag ratio performance as well as having a positive effect on the hydrodynamic performance of the hydrofoil. Guo *et al.* (2019) investigated two types of guide vanes, including original guides vane and waveguide vanes with bio-inspired leading-edge protuberances. By comparison, the latter effectively improved the hump characteristics of the pump-turbine. Li *et al.* (2019) examined the role of sinusoidal tubercles trailing edges in centrifugal pumps. They found that the hydraulic performance of sinusoidal tubercles trailing edges was superior, and the pressure pulsation and energy loss of the pump were minimized.

Inspired by bionics, we designed three sinusoidal tubercles volute tongues. The influence of the sinusoidal tubercle volute tongues on the pressure pulsation was investigated, and the flow structure and enstrophy of the four pumps were analyzed, aiming to minimize pressure pulsation, maximize hydraulic performance and reduce the energy dissipation in centrifugal pumps. It provides a feasible solution to reduce the vibration noise in the centrifugal pump and improve the stability and the working conditions of the pump.

2. MAIN PUMP GEOMETRY

2.1 Test Model Pump

In this paper, the experimental results of Kelder *et al.* (2001) were used for the validation of this study. The flow rates of the experiments were 82.5%, 100%, and 112% of the design flow rate respectively. The Laser Doppler Velocimeter (LDV) measurement system was used for velocity measurement. U-tube manometers were used to obtain values of the static pressure. The measurement locations of the velocity and static pressure data are shown in Fig. 1. The impeller is composed of 7 blades, and the blade angle relative to the radial direction is constant at 70 degrees, whose thickness is constant at 2mm. The volute tongue is cylindrical with a diameter of 2 mm. The design flow rate Q_d and the angular velocity

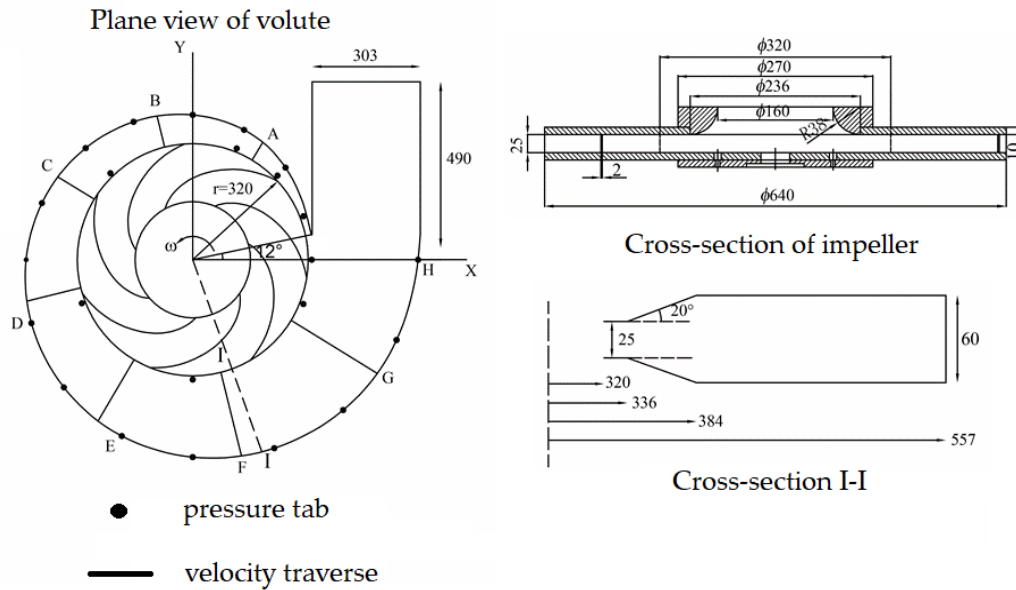


Fig. 1. Pump geometry of the centrifugal pump and the locations of velocity and static pressure measurement.

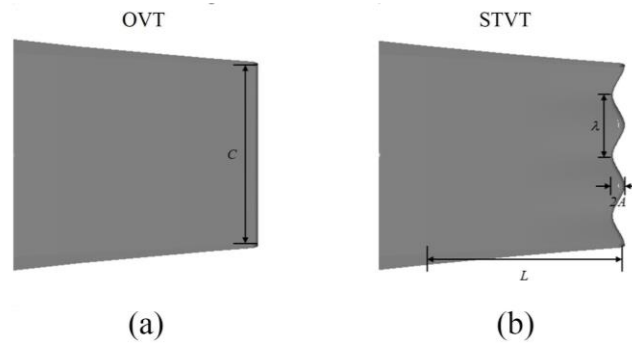


Fig. 2. Differences between two types of tongues: (a) OVT; (b) STVT.

V_ω are $28.8\text{m}^3/h$ and 4.2rad/s . The main geometric parameters of the pump used by Kelder *et al.* (2001) are shown in Fig. 1 and Table 1.

Table 1 Parameters for the test centrifugal pump

Parameters	Sign	Value
Nominal flow coefficient	φ_d	0.15
Nominal head coefficient	ψ_n	0.124
Inlet diameter of impeller(mm)	d_1	320
Outlet diameter of impeller(mm)	d_2	640
Blade width at exit(mm)	b_2	25
Blade angle at exit ($^\circ$)	β_2	30
Blade number	Z	7
Volute tongue diameter(mm)	d_3	336
Inlet width of volute(mm)	b_3	25

2.2 Volute Tongue

Three bionic volute tongues were designed based on the original volute. Figure 2 shows the difference between the Original Volute Tongue (OVT) and three newly designed Sinusoidal Tubercle Volute Tongues (STVT). The parameters of the three bionic tongues are shown in Table 2. OVT is the original volute tongue, which is a border-radius. The vortexes shedding from the OVT profile are intensive. The STVT only exists on the volute tongue. The number of tubercles in the bionic volute tongue was three (STVT-1), four (STVT-2), and five (STVT-3), respectively. There are sinusoidal grooves near the tongue, of which the length of the longitudinal extension length is L . And the groove depth gradually decreases from $2A$ to zero along the tongue profile line. As shown in Fig. 1, λ is the sinusoidal wavelength, indicating the spacing of sinusoidal nodules. A is the amplitude of the sinusoid, which is half the height of the sinusoidal tubercle. According to the width of the volute tongue ($C = 30\text{mm}$), the values of L and A are 15 mm and 2 mm, and the values of λ

in three sinusoidal tubercle volute tongues are 10mm, 7.5mm and 6mm, respectively. In the design process, the essential parameters of the four volutes are the same.

Table 2 Parameters for the bionic tongues

	The number of sinusoidal tubercles	λ	A	C	L
STVT-1	3	10	2	30	15
STVT-2	4	7.5	2	30	15
STVT-3	5	6	2	30	15

3. NUMERICAL INVESTIGATION

3.1 Numerical Method

The commercial software CFX 16.0 was used to calculate the steady and unsteady constant numerical simulation of the total flow field in this study. The static pressure was set at the inlet of the pump and the mass flow rate was set at the outlet as the boundary conditions. Both of these values were proposed by *Kelder et al. (2001)*. The impeller was set to a rotating computational domain and the rest were stationary computational domains. This article ignored the effect of roughness, that is, all the walls were smooth without sliding. The turbulent intensity of 5% was set in the inlet boundary. The high-resolution scheme was selected for the advection scheme, and the second-order was used for the turbulence numeric. Taking the rotation of the impeller 1° as a time step, and every calculation of 360 steps was one cycle of the impeller rotation. The root mean square (RMS) was set to 10^{-5} to converge the result.

In the steady-state simulation, we chose the shear stress transfer (SST) $k-\omega$ model to obtain the head and coefficient of the four pumps. While in the transient simulation, the detached-eddy simulation (DES) model based on the SST $k-\omega$ model was applied to capture the rest of the datum to compare with the experimental data and optimize the analysis of the bionic tongues. In the transient simulation, in order to obtain fast convergence results, the steady calculation results were used as the initial flow conditions of the un-steady calculation DES model. In order to obtain stable operation results, we used CFX software to simulate the transient state of 12 revolutions, and only retained the data of the last 4 revolutions to analyze the pressure fluctuation.

3.2 Computational Mesh

The entire calculation area was divided into three parts, namely the impeller, the volute, and the inlet extension. In order to ensure the accuracy and efficiency of the simulation calculation, the entire calculation domain used the structured hexahedral

mesh generated by ANSYS-ICEM 16.0 software. The mesh of the entire pump and the boundary layer mesh of the regions in three bionic tongues and the impeller blade wall surface were shown in Fig. 3. Four types of grids were used for grid independence test, as shown in Table 3. The results show that the grid size has little effect on the head coefficient and efficiency of pumps. Therefore, case 3 was chosen for the following transient numerical simulation calculations. The total number of grids in the computing domain was 4.49 million, and the y^+ value (7.2) of the turbulence model also met the requirements. The average y^+ value of the impeller was about 7.7, and the average y^+ value of the volute was 6.9.

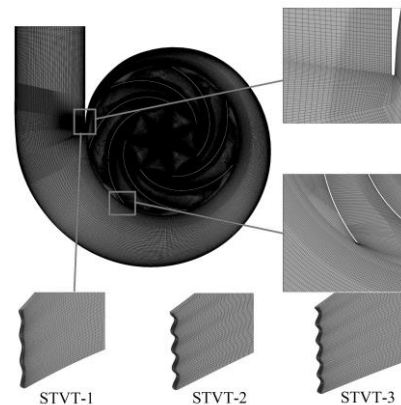


Fig. 3. Structured hexahedral mesh of the impeller and volute.

Table 3 Grid convergence for four different grids

case	1	2	3	4
Nodes (10^6)	2.24	3.48	4.49	5.93
Mean y^+	16.3	10.5	7.2	5.8
Head coefficient ψ^*	0.1072	0.1065	0.1061	0.1057
Efficiency η	84.5	83.8	83.4	82.9

3.3 Monitoring Points Arrangement

In this study, 10 monitoring points were set in the middle cross-section of the volute channel, which was used to obtain the pressure fluctuation signal and turbulent kinetic energy signal of the flow channel in the volute and tongue region. At the same time, in order to accurately study the rotor-stator interaction between the impeller and the volute tongue in the centrifugal pump, four monitoring points T1-T4 were set near the tongue. Figure 4 shows the detailed location distribution.

3.4 Validation of Calculation Results

The pressure values were dimensionless to represent the pressure distribution in the pump

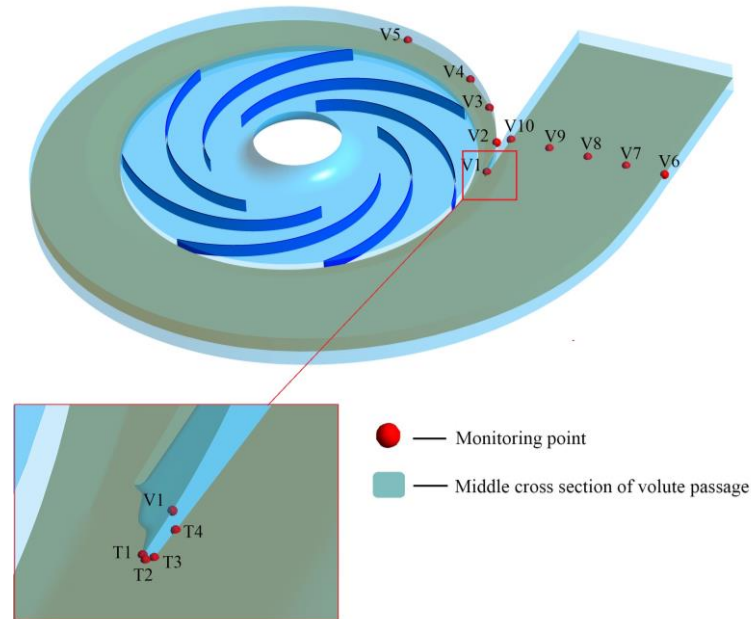


Fig. 4. Location of monitoring points.

cavity of the four models. Δp is the static pressure coefficient, which is defined as:

$$\Delta p = \frac{p - p_{inlet}}{\rho(V_\omega r_{TE})^2} \quad (1)$$

where V_ω is the angular velocity of the pump, r_{TE} is the blade tip radius and ρ is the fluid density.

Fig. 5 shows the comparison between the actual experimental head curve and the numerical simulation head curve at different flows. The simulated head and the actual head in the figure basically coincide with the small flow condition. While when $Q/Q_d > 1.0$, there is a small deviation. Therefore, it shows that the simulated characteristic curve is in good agreement with the experimental results, which verifies the accuracy of the current numerical method.

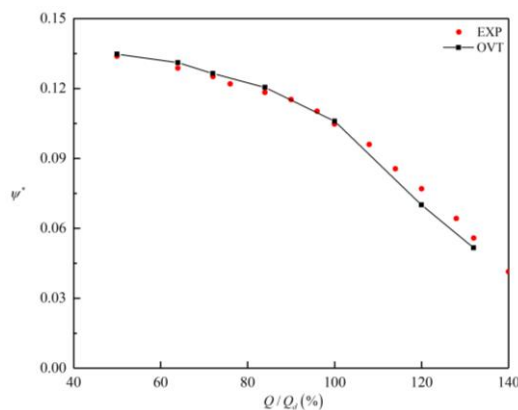


Fig. 5. Comparison between numerical and experimental values of the head coefficient under different flow rates.

The comparison between the numerically simulated static pressure and the experimental static pressure at the design flow rate was displayed in Fig. 6, where Fig. 6(a) is the static pressure around the impeller and Fig. 6(b) is the static pressure on the outer wall of the volute. The numerical simulation of the static pressure distribution agrees well with the experimental data. This result also verifies the calculation accuracy of existing numerical methods. Fig. 7 presents the comparison of the time-averaged radial and circumferential velocity components with the experimental data. At the design flow rate, four traverses (A, D, F, H) along the centerline of the volute (Fig. 1) were compared. The scaled local coordinate along the traverse is denoted by r^* ranging from 0 at the impeller outer radius to 1 at the volute wall. Velocities are scaled with blade tip velocity. The deviation of the simulation results from the experimental data is very small. This shows that the variation tendency of the simulation result is consistent with the measured result, that is, the value of the numerical simulation is in line with the conditions.

4. RESULTS AND ANALYSIS

4.1 Performance Analysis of Four Test Pumps

Figure 8 shows the head coefficient and efficiency curves of four volute tongues profiles model pump. is the head coefficient, which is defined as follows:

$$\psi^* = \frac{gH}{(V_\omega d_2)^2} \quad (2)$$

The head coefficient decreases with the increase in flow rate. However, the efficiency increases first

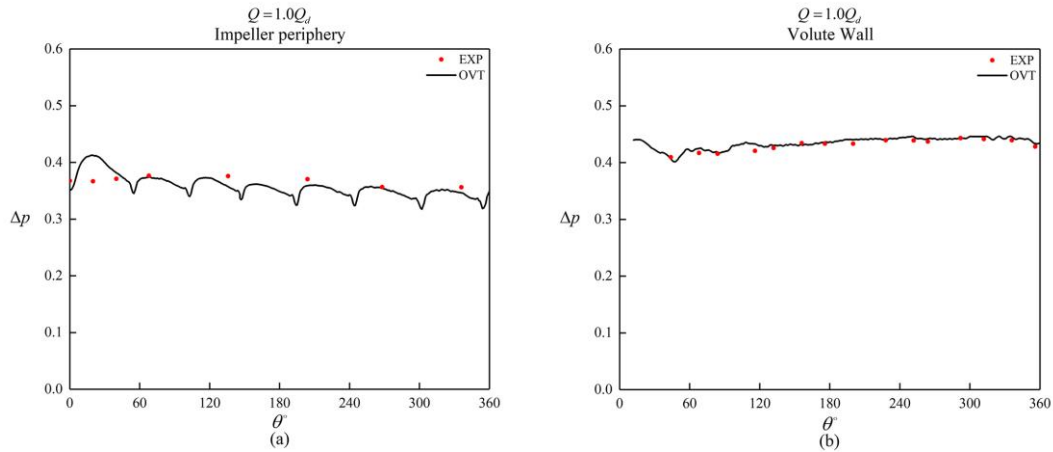


Fig. 6. Comparison of predicted and measured non-dimensional static pressure distributions: (a) impeller periphery; (b) volute wall.

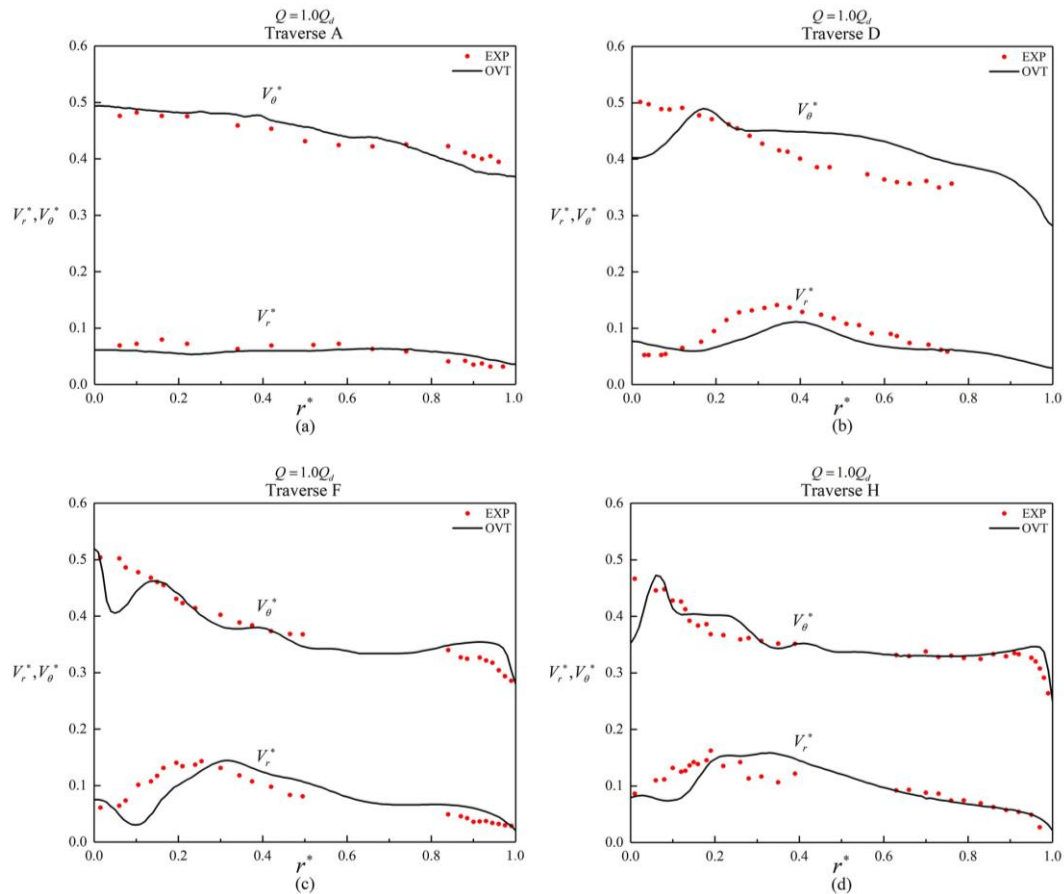


Fig. 7. Non-dimensional radial and circumferential velocities in the volute along different traverses at design flow rate: (a) Traverse A; (b) Traverse D; (c) Traverse F; (d) Traverse H.

and then de-creases, reaching the maximum at the designed flow rate. Under the condition of a small flow rate, there is a slight difference in the hydraulic performance of four pumps. In the designed flow conditions, the head of the four pumps is basically the same, and the efficiencies of the STVT profiles are higher than the OVT profile. Under high flow conditions, the head of the STVT-

2 profile is higher than that of the other three pumps, while the head of the STVT-3 profile is the low-est. However, the efficiencies of all bionic tongues are higher than that of the OVT profile. At the design flow rate, the efficiency of the three bionic pumps is increased by 0.5% (STVT-1), 1.5% (STVT-2), 0.9% (STVT-3), respectively. When $Q/Q_d = 1.32$, the improved efficiency is 1%

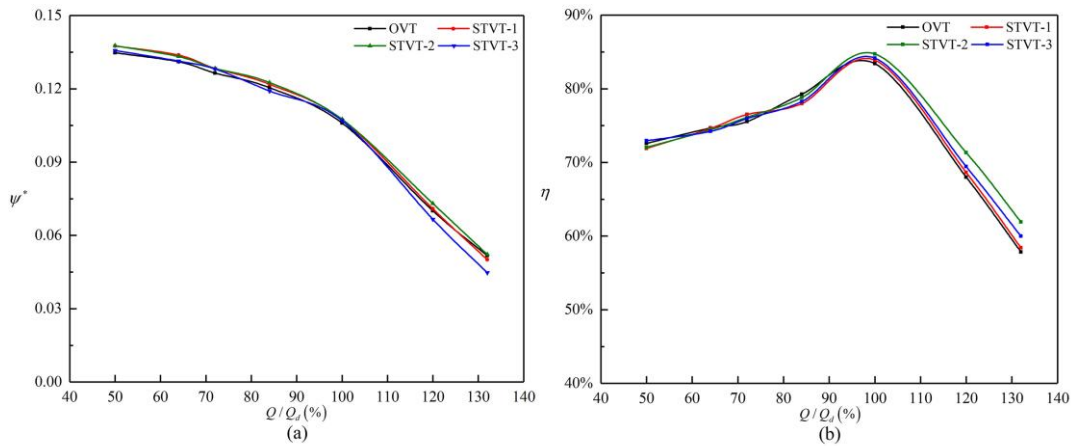


Fig. 8. Comparison of predicted performance curves with different tongues: (a) head coefficient; (b) efficiency.

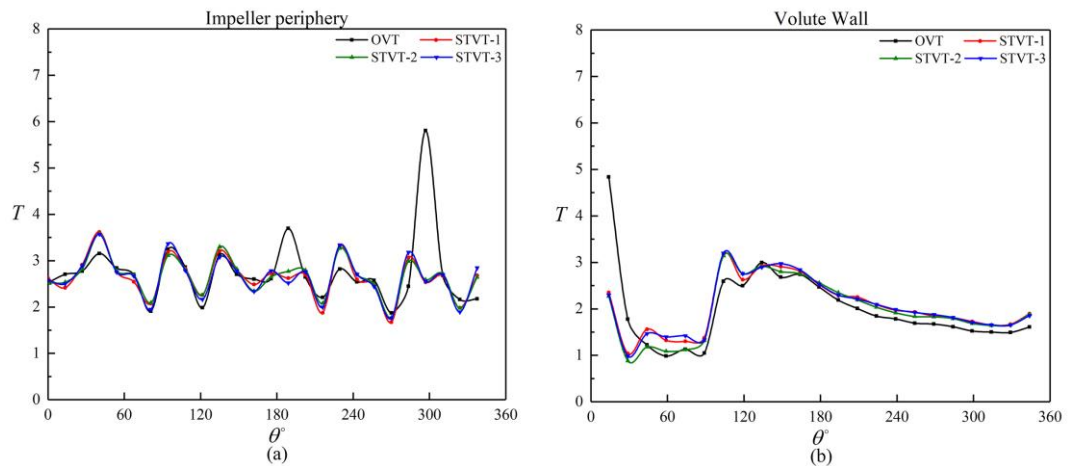


Fig. 9. Turbulent kinetic energy distribution: (a) Impeller periphery; (b) Volute wall.

(STVT-1), 6.8% (STVT-2), 3.6% (STVT-3) respectively. And the efficiency of the STVT-2 profile is the highest. The increase of the head and efficiency is due to the moderate flow of fluid in the bionic tongues. Obviously, the design of the tongue with four sinusoidal tubercles is superior.

Figure 9 demonstrates the distribution of turbulent kinetic energy on the impeller periphery and the volute wall. It shows that the changing trend of the turbulent kinetic energy of the STVT profiles on the impeller periphery is roughly the same, but slightly lower than the OVT profile. The difference among the OVT profile and the STVT profiles is particularly obvious around 180° and 300° . In Fig 9(b), the turbulent kinetic energy curve of the bionic tongues is much lower than the OVT profile as less than 30° , with the STVT-2 profile being the lowest. When it is greater than 60° , the variation tendency of the turbulent kinetic energy of the four model pumps is consistent, and the turbulent kinetic energy of the OVT profile is slightly higher than that of the bionic tongue. Under various working conditions, the turbulent energy value near the

tongue changed abruptly. This is the result of the strong rotor-stator interaction between the impeller and the volute (Zhang *et al.* 2016). Therefore, the turbulence of the fluid near the tongue is the strongest, and it also causes large energy loss. In the figure, the turbulent kinetic energy of the STVT profiles near the tongue is significantly lower than the OVT profile, indicating that the bionic tongues reduce turbulent kinetic energy near the tongue. This also proves that the bionic tongues (especially the STVT-2 profile) improve the hydraulic performance of the pump.

Enstrophy is a new term that appeared in hydrodynamics within the last thirty years. Enstrophy does not have the dimension of energy but is proportional to the rate of energy dissipation. To further study the positive influence of the bionic tongues on the performance of the centrifugal pump, the total enstrophy equation of the flow field is introduced as:

$$\Omega(t) = \frac{1}{2} \int \rho \omega^2 dv \quad (3)$$

It is the volume integral of scalar $\omega^2/2$. ω is the vorticity of the flow field, ρ is the density. This equation can be used to determine whether the flow field has rotation and the degree of rotation. Obviously, taking the square of the vorticity avoids the vorticity of the closed vortex tube canceling each other out during integration, which makes $\Omega(t)=0$ a sufficient and necessary condition for the flow field to have no rotation. Meanwhile, by integrating the dissipation function of the flow field, we found that the total dissipation of mechanical energy is directly related to the total enstrophy.

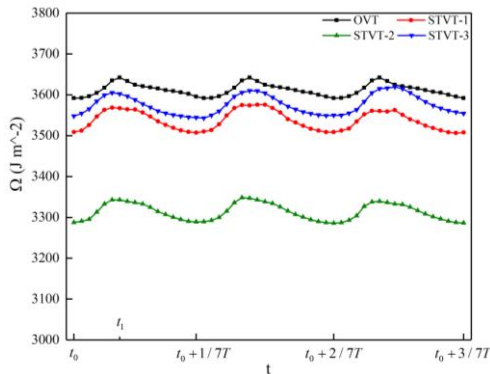


Fig. 10. Total enstrophy of the flow field in volute of four pumps.

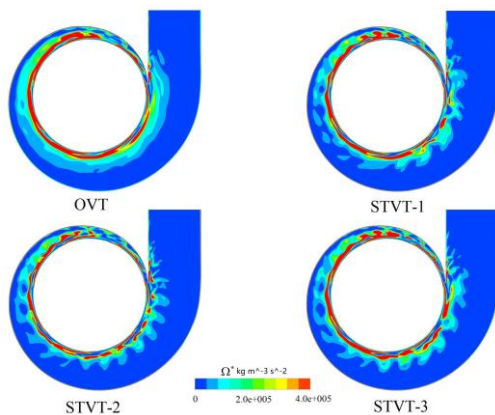


Fig. 11. Enstrophy distribution at t_1 of four pumps.

Since the bionic tongue has little effect on the enstrophy of the impeller and the inlet extension, we only analyze the total enstrophy in the volute. Figure 10 shows the curve of the total enstrophy in the volute of the flow field of four pumps with time. t_0 is the time at the beginning of the twelfth revolutions. The statistical time is $3/7T$. Therefore, there are three similar peaks and valleys in the figure. The changing trend of the four pumps is consistent. But the enstrophy of the flow with STVT profiles is significantly lower than the OVT profile. And there is a slight difference among STVT-1 profile, STVT-3 profile and OVT profile. The reduction in the enstrophy among them is less than 1.5%. The enstrophy of flow with the STVT-2 profile is the lowest, approximately 8% lower.

Figure 11 shows the enstrophy distribution per unit volume of four pumps at t_1 ($\Omega^* = 1/2\rho\omega^2$). Obviously, the region of the enstrophy per unit volume in the STVT-2 profile is the smallest. This shows that the STVT profiles effectively minimize the total enstrophy of the flow field and the dissipation of mechanical energy. At the same time, the optimized design of the tongue with four sinusoidal tubercles reduces the energy dissipation of the centrifugal pump during operation. This also has a positive effect on improving pump performance. It proves that the optimized design of the STVT-2 profile has achieved the expected result.

4.2 Pressure Analysis of Four Test Pumps

Figure 12 shows the instantaneous pressure distribution of the middle cross-section of the impeller and volute of four pumps under the design conditions. The curves of the static pressure of the STVT profile are always lower than the OVT profile. In the impeller periphery, the differences in static pressure are larger near the upstream of the tongue, reaching the maximum around 180° . As demonstrated in Fig. 12(b), the trend of the static pressure distribution of the STVT profiles is basically the same as that of the OVT profile. However, the pressure difference maximizes near the tongue. Then, the pressures at the monitoring points of the four pumps tend to be consistent. The bionic tongue reduces the rotor-stator interaction between the impeller and the volute, as well as reduces the static pressure at the tongue.

During the analysis of pressure spectra, we introduced the dimensionless pressure pulsation coefficient C_p to process the pressure signal, which is defined as follows:

$$C_p = \frac{(p_i - \bar{p})}{\frac{1}{2}\rho u_2^2} \quad (4)$$

where p_i represent the pressures sample values at each time step. \bar{p} is the time-average pressure. u_2 is the circumferential speed at the impeller exit.

The DES model was used in transient-state simulations to capture pressure pulsation signals and flow patterns, which clearly explains how the STVT profiles affect pulsations. To obtain steady pressure pulsation signals, the pressure fluctuation curve of the two periods at the monitoring point T2 is shown in Fig. 13. The pressure pulsation coefficient of different tongues positions changes periodically, and seven different peaks and valley appear within a cycle of the impeller rotation. This is caused by 7 evenly distributed blades of the impeller. At the monitoring point T2, the changing trend of the pressure fluctuation coefficient of the four pumps is consistent. The pressure signals of the pumps with the bionic tongue are lower than the OVT profile, and the STVT-2 profile is the lowest. Obviously, the model pumps with bionic tongues have better pressure stability, which effectively reduces the pressure pulsation.

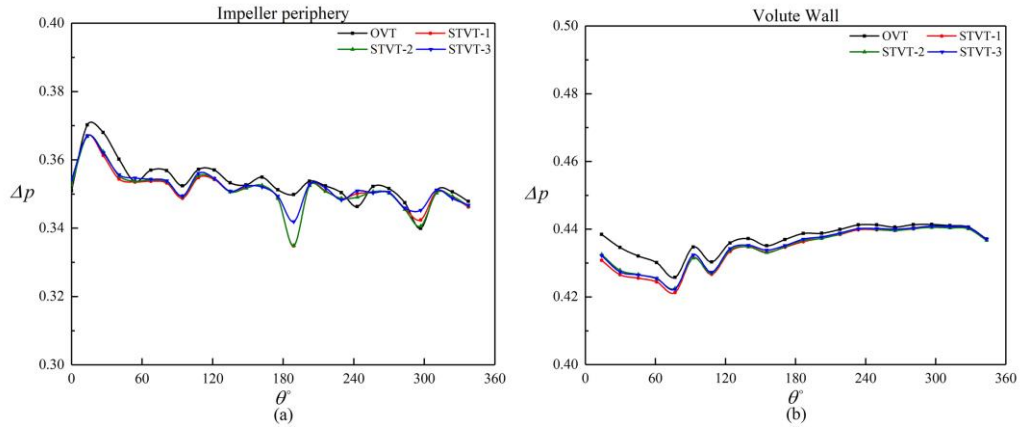


Fig. 12. Pressure distribution of four model pumps: (a) Impeller periphery; (b) Volute wall.

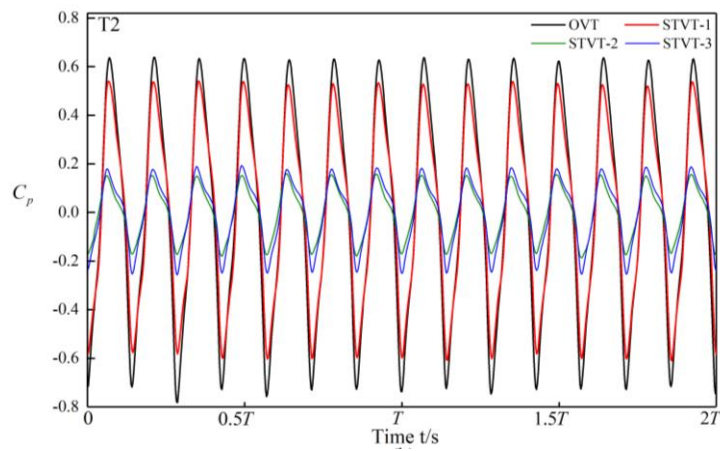


Fig. 13. Time-domain pressure pulsation at point T2.

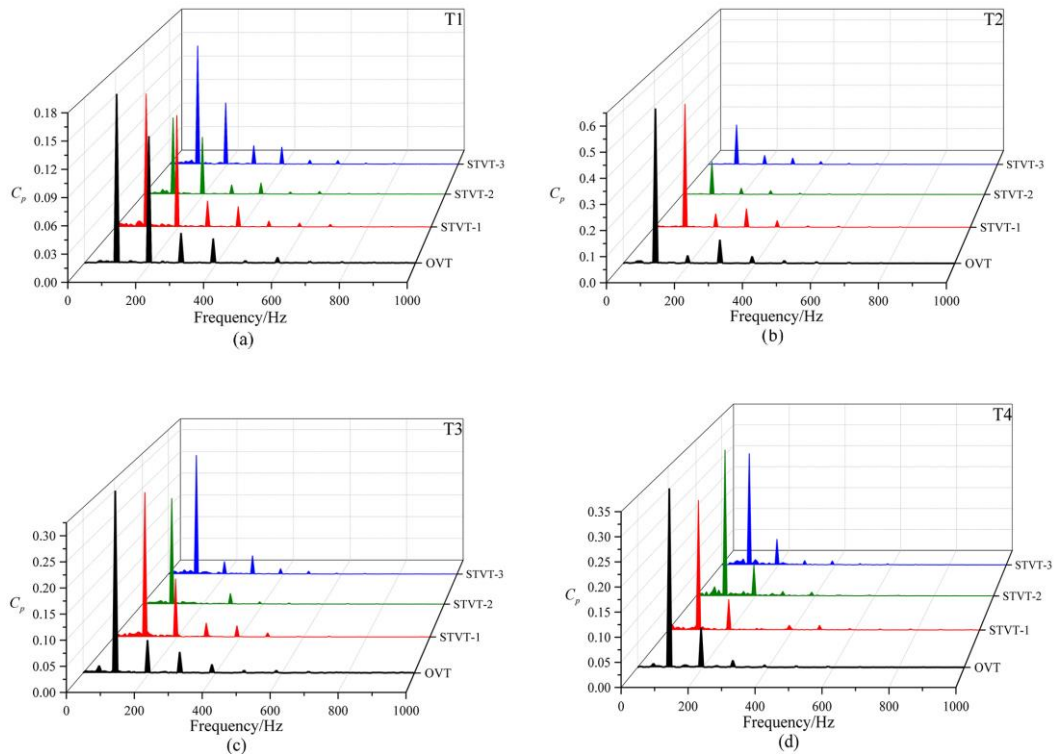


Fig. 14. Frequency-domain pressure pulsations at points T1-T4.

For a better analysis of the influence of the bionic tongue on the pressure fluctuation, the fast Fourier transform (FFT) was used to convert the collected pressure pulsation time-domain signal into a frequency spectrum. The pressure value of the last three revolutions at the design flow is selected. The interaction between the impeller and the volute mainly occurs in the tongue area. The monitoring points T1-T4, near the tongue, were selected for frequency domain analysis, as shown in Fig. 14. The pulsation amplitude at the blade passing frequency (BPF) is dominant in the frequency spectrum, and the amplitude at the double BPF is much smaller than the amplitude in BPF. Due to the rotor-stator interaction between the impeller and the tongue, the monitoring points T1-T4 near the tongue have a large pulsation amplitude at the BPF and the double BPF. The magnitudes of monitoring points near the tongue (T1-T4) are greater. The magnitude of monitoring point T2 of the OVT profile is the largest, whose value is 0.62. The farther away from the tongue, the smaller the magnitude. By comparing the pressure pulsation amplitudes of the four model pumps at the same monitoring point, it is observed that the pressure amplitudes of the bionic tongues at the BPF and the double BPF have different degrees of decrease. In general, the STVT profiles have lower Frequency-domain pressure pulsations. And the difference in pressure amplitude between the monitoring points T1-T4 near the tongue is more obvious.

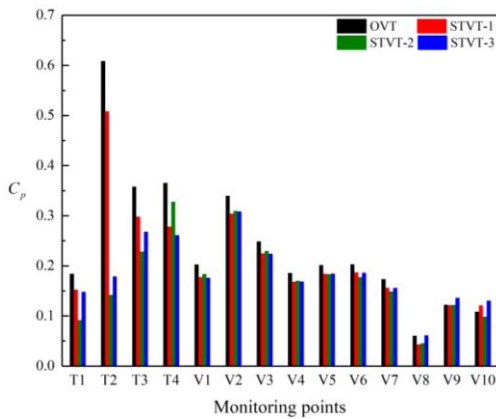


Fig. 15. Pressure amplitude at various monitoring points in BPF.

Figure 15 shows the comparison of the pressure coefficient in BPF among four pumps. The reductions between three bionic pumps and the original pump are shown in Table 4. It can be seen from the figure that the amplitudes of the points T1-T4 near the tongue in BPF are the largest. This is because the area near the tongue is more affected by the rotor-stator interaction between the impeller and the volute. And by comparing the four curves, the pressure amplitudes in pumps with STVT profiles are lower than the OVT profile. The difference is largest at T1-T4 and smallest at V6-V10. Meanwhile, the pressure amplitude of the STVT-2

profile is the lowest in BPF. The reductions of the average pressure pulsation at the monitoring points are 13.3% (STVT-1), 20.6% (STVT-2), and 16.2% (STVT-3), respectively. The results show that STVT profiles effectively minimize pressure pulsation and reduce the impact of the rotor-stator interaction. And the pump with four sinusoidal tongues performs the best.

Table 4 the reduction in BPF among three pumps with bionic tongue

	Reduction (%)		
	STVT-1	STVT-2	STVT-3
T1	17.34	50.2	19.53
T2	16.46	76.65	70.61
T3	16.76	36.21	25.18
T4	23.83	10.33	28.56
V1	12.53	9.38	13.02
V2	10.46	8.83	9.19
V3	9.67	7.62	9.98
V4	9.39	8.26	9.18
V5	8.54	8.91	8.4
V6	8.06	12.64	8.46
V7	10.03	14.06	9.92
V8	28.5	24.68	-1.36
V9	0.72	0.39	-0.11
V10	-11.55	9.27	-0.20

4.3 Flow Structures of Four Test Pumps

In order to understand the mechanism of the bionic tongue in improving the pump performance and pressure pulsation, and to better observe the shape of the shedding vortex near the tongue, the distribution of vortex cores in the tongue area of four pumps is presented in Fig. 16.

Compared with the original model pump, the area occupied by the distribution of the vortex cores of the STVT profiles is greatly reduced. The large vortex in the OVT profile has been changed to some small vortexes in the STVT profiles, and the total amount is greatly reduced. The wide cluster strip-shaped vortex is separated into several small strip-shaped shed vortexes by the sinusoidal tubercles. The region of the vortex core and energy is reduced, and the rotor-stator interaction generated by the vortex shedding is weakened. There is the smallest region of vortex core distribution in the STVT-2 profile. Controlling the vortex shedding by changing the shape of the volute tongue is acceptable, which has a positive effect on the stability of the pressure and the performance of the pump.

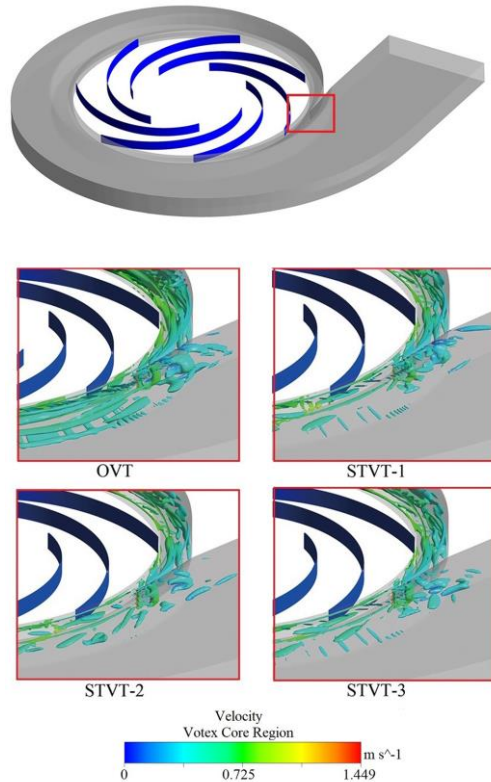


Fig. 16. Vortex core distributions (Q-criterion) in the volute tongue region.

5. CONCLUSIONS

In this paper, the numerical study of the centrifugal pumps with or without the STVT was conducted. The effects of four tongue shapes on pressure pulsation, performance, frequency domain, and enstrophy are discussed, and conclusions are drawn as follows.

The head and efficiency of the pump with the STVT profile are slightly higher. At the design flow rate, the efficiencies of the three bionic pumps are increased by 0.5% (STVT-1), 1.5% (STVT-2), 0.9% (STVT-3), respectively. The turbulent kinetic energy and enstrophy are lower in the pump with STVT profiles. The STVT-2 profile performs the best. The reduction of enstrophy in the STVT-2 profile is 8%, the others are less than 1.5%. Therefore, the energy dissipation of the STVT profiles is lower, which reduces the loss of mechanical energy and has a positive effect on improving the performance of the pump.

By comparing the four model pumps, the pressure pulsations in the pumps with the STVT are lower in time and frequency domains at each monitoring point, especially near the tongue, which reduces the rotor-stator interaction between the impeller and the volute. The reductions of the average pressure pulsation at the monitoring points are 13.3% (STVT-1), 20.6% (STVT-2), and 16.2% (STVT-3), respectively. Among them, the STVT-2 profile has the lowest pressure pulsation.

By analyzing the vortex core distribution of the four models, the STVT minimize the vortex of the entire computing region and divide the large vortex shedding near the tongue into several small vortices, and reduce the size of the vorticity, making the flow inside the pump more stable.

ACKNOWLEDGEMENTS

The present work is financially supported by the National Natural Science Foundation of China (Grant No. 51676173), the Key R & D Program of Zhejiang Province (Grant No. 2020C03081), the National Basic Research Program of China (Grant No. 613321), and 521 Talents Fostering Program Funding of Zhejiang Sci-Tech University of China. The supports are gratefully acknowledged.

REFERENCES

- Bai, L., L. Zhou, C. Han, Y. Zhu and W. Shi (2019). Numerical Study of Pressure Fluctuation and Unsteady Flow in a Centrifugal Pump. *Processes* 7, 354.
- Cheng, H. Y., X. R. Bai, X. P. Long, B. Ji, X. X. Peng and M. Farhat (2020). Large eddy simulation of the tip-leakage cavitating flow with an insight on how cavitation influences vorticity and turbulence. *Applied Mathematical Modelling* 77, 788-809.
- Gao, B., N. Zhang, Z. Li, D. Ni and M. Yang (2016). Influence of the Blade Trailing Edge Profile on the Performance and Unsteady Pressure Pulsations in a Low Specific Speed Centrifugal Pump. *Journal of Fluids Engineering* 138(5), 51106.
- Gu, Y., J. Pei, S. Yuan and W. Wang (2019). Clocking effect of vaned diffuser on hydraulic performance of high-power pump by using the numerical flow loss visualization method. *Energy* 170(MAR.1), 986-997.
- Guo, Z. W., C. H. Wang, Z. D. Qian, X. W. Luo and W. P. Xia (2019). Suppression of hump characteristic for a pump-turbine using leading-edge protuberance. *Proceedings of the Institution of Mechanical Engineers Part A Journal of Power and Energy*, 095765091985463.
- Hua, X., C. Zhang, J. Wei, X. Hu and H. Wei (2019). Wind turbine bionic blade design and performance analysis. *Journal of Visual Communication and Image Representation* 60, 258-265.
- Huang, B., S. Qiu, X. Li, Q. Wu and G. Wang (2019). A review of transient flow structure and unsteady mechanism of cavitating flow. *Journal of Hydrodynamics* 31(2), 429-444.
- Kelder, J., R. Dijkers, B. Esch and N. Kruyt (2001). Experimental and theoretical study of the flow in the volute of a low specific-speed pump. *Fluid Dynamics Research* 28(4), 267-280.

- Kergourlay, G., M. Younsi, F. Bakir and R. Rey (2007). Influence of Splitter Blades on the Flow Field of a Centrifugal Pump: Test-Analysis Comparison. *International Journal of Rotating Machinery* 2007, 1-13.
- Khalifa, A. E., A. M. Al-Qutub and R. Ben-Mansour (2011). Study of Pressure Fluctuations and Induced Vibration at Blade-Passing Frequencies of a Double Volute Pump. *Arabian Journal for Science and Engineering* 36(7), 1333-1345.
- Li, B. W., X. J. Li, X. Q. Jia, F. Chen and H. Fang (2019). The Role of Blade Sinusoidal Tubercle Trailing Edge in a Centrifugal Pump with Low Specific Speed. *Processes* 7, 625.
- Luo, X., W. Wei, B. Ji, Z. Pan, W. Zhou and H. Xu (2013). Comparison of Cavitation Prediction for a Centrifugal Pump with or without Volute Casing. *Journal of Mechanical Ence and Technology* 27(6), 1643-1648.
- Majidi, K. (2005). Numerical study of unsteady flow in a centrifugal pump. *Journal of Turbomachinery* 127(2), 363-371.
- Shi, W., M. Atlar, R. Norman, B. Aktas and S. Turkmen (2016). Numerical optimization and experimental validation for a tidal turbine blade with leading-edge tubercles. *Renewable Energy* 96(pt. a), 42-55.
- Shim, H., A. Afzal, K. Kim and H. Jeong (2016). Three-objective optimization of a centrifugal pump with double volute to minimize radial thrust at off-design conditions. *Proceedings of the Institution of Mechanical Engineers Part A: Journal of Power and Energy* 230(6), 598-615.
- Si, Q., P. Dupont, A. Bayeul-Lainé, A. Dazin, O. Roussette and G. Bois (2016). Static Pressure Recovery Analysis in the Vane Island Diffuser of a Centrifugal Pump. *Journal of Mechanical Science and Technology* 30(2), 549-556.
- Solis, M., F. Bakir, S. Khelladi and R. Noguera (2011). Numerical Study on Pressure Fluctuations Reduction in Centrifugal Pumps: Influence of Radial Gap and Splitter Blades. *Isrn Mechanical Engineering* 2011(2), 1-14.
- Spence, R. and J. Amaral-Teixeira (2008). Investigation into pressure pulsations in a centrifugal pump using numerical methods supported by industrial tests. *Computers and Fluids* 37(6), 690-704.
- Spence, R. and J. Amaral-Teixeira (2009). A CFD Parametric Study of Geometrical Variations on the Pressure Pulsations and Performance Characteristics of a Centrifugal Pump. *Computers and Fluids* 38(6), 1243-1257.
- Xiao, Y. X., D. G. Sun, Z. W. Wang, J. Zhang and G. Y. Peng (2012). Numerical analysis of unsteady flow behaviour and pressure pulsation in pump turbine with misaligned guide vanes. *Iop Conference* 15(3), 32043.
- Xue, G., Y. Liu, M. Zhang and H. Ding (2016). Numerical Analysis of Hydrodynamics for Bionic Oscillating Hydrofoil Based on Panel Method. *Applied Bionics and Biomechanics* 2016, 6909745.
- Yang, Z. X., G. S. Li, L. Song and Y. F. Bai (2017). Effects of setting angle and chord length on performance of four blades bionic wind turbine. *Iop Conference* 93, 12041.
- Ye, L., S. Yuan, J. Zhang and Y. Yuan (2012, July). Effects of Splitter Blades on the Unsteady Flow of a Centrifugal Pump. *Proceedings of the ASME Fluids Engineering Division Summer Meeting*, Rio Grande, Puerto Rico, USA, 8-12.
- Zhang, N., M. Yang, B. Gao, Z. Li and D. Ni (2015). Experimental Investigation on Unsteady Pressure Pulsation in a Centrifugal Pump with Special Slope Volute. *Journal of Fluids Engineering* 137(6), 61103.
- Zhang, N., M. Yang, B. Gao, Z. Li, and D. Ni (2016). Investigation of rotor-stator interaction and flow unsteadiness in a low specific speed centrifugal pump. *Strojniški vestnik-Journal of Mechanical Engineering* 62(1), 21-31.